Colloids and Surfaces A: Physicochemical and Engineering Aspects 733 (2026) 139278

Contents lists available at ScienceDirect

Colloids and Surfaces A: Physicochemical and Engineering Aspects

journal homepage: www.elsevier.com/locate/colsurfa

Unraveling interference contributions to light scattering from concentrated colloids: A numerical study using density expansion

Hiroyuki Fujii *, Sou Sasaki, Ryuga Sawada, Kazumichi Kobayashi, Masao Watanabe

Division of Mechanical and Space Engineering, Faculty of Engineering, Hokkaido University, Kita 13 Nishi 8, Kita-ku, Sapporo, 060-8628, Hokkaido, Japan

HIGHLIGHTS

- Analytic decomposition of interference in light scattering via density expansion.
- Calculations of the scattering coefficients using the electromagnetic theory.
- Small particle size case enhances the multiple interference in the coefficients.
- This decomposition approach unveils hidden constructive interference.
- Constructive interference correlates with the effective attraction between particles.

GRAPHICAL ABSTRACT

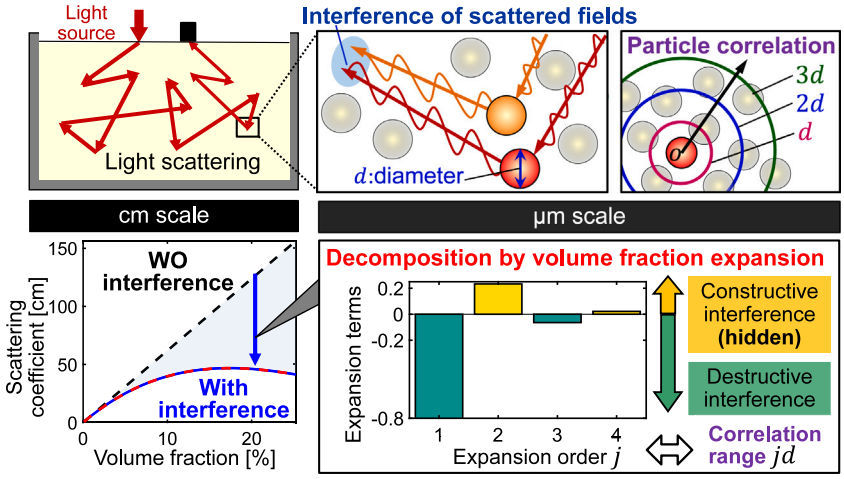

ARTICLE INFO

Keywords:
Light scattering properties
Interference effect
Dependent scattering theory
Density expansion approach
Pair correlation between particles

ABSTRACT

In dense colloidal suspensions, far-field interference between electric fields scattered by particles significantly influences light scattering properties. Previous studies using dependent scattering theory (DST), based on the first-order solution of the Foldy–Lax equations, have shown that destructive interference affects the scattering properties via the static structure factor. Meanwhile, the contributions of multiple interference and the relationship between interference and particle correlation remain unclear. We aim to clarify the interference effects and their relationship using a density expansion approach, which allows us to decompose the multiple interference contributions. We calculated the two scattering coefficients using the DST and the expansions with hard-sphere interaction in the volume fraction range up to 25% and the optical wavelength range of 600–1000 nm. Our numerical calculations showed that for particle diameters larger than approximately 300 nm, the second-order expansion for the reduced scattering coefficient agrees well with the DST results. This result reflects the destructive interference induced by the excluded volume between particles. For the scattering coefficient, the third-order expansion agrees with the DST results in the larger-diameter region. This agreement reveals a hidden constructive-interference contribution driven by an effective attractive interaction, even in the absence of any direct attractive force. For smaller diameters, higher-order expansions are necessary to accurately reproduce the DST results, as multiple interference contributions are involved. For the scattering coefficient, odd-order terms of expansion correspond to destructive interference, while even-order terms

* Corresponding author.
E-mail address: fujii-hr@eng.hokudai.ac.jp (H. Fujii).

https://doi.org/10.1016/j.colsurfa.2025.139278
Received 6 October 2025; Received in revised form 14 December 2025; Accepted 15 December 2025
Available online 18 December 2025

correspond to constructive interference. In contrast, the correspondence in the reduced scattering coefficient is more complex and depends on both particle diameter and wavelength. Our findings provide fundamental knowledge for developing nanotechnology to evaluate colloidal particle properties non-destructively using scattered light.

1. Introduction

Colloidal suspensions are essential and found in various nano- and micro-scale engineering and scientific fields [1–3], such as slurries in chemical engineering, colloidal photocatalysts in environmental remediation, and milk in food science. High concentrations are significantly demanded in various industries, such as for improving product quality and reducing transport costs through the weight reduction of suspensions [4,5]. High concentrations are also crucial for physicochemical phenomena, including glass transition and its quasi-universality [6,7].

Light scattering techniques have been extensively developed to retrieve the physicochemical properties (i.e., viscosity) [8] and colloidal particle properties (i.e., nano- and micro-particle size, and agglomeration degree) [9–12]. In a light-scattering process, the direction of the scattered light frequently changes due to colloidal particles (scatterers). Meanwhile, most developed techniques require sample dilution, where the volume fraction is less than approximately 5%. Photon density wave spectroscopy can potentially retrieve the properties without dilution [13]. To further develop the optical method, quantitative understanding of light scattering in dense suspensions needs to be clarified [14].

Light scattering properties, one of the physicochemical properties, quantify the strength of light scattering. For example, the scattering coefficient represents the inverse mean free path of photons [15]. Experimental and theoretical studies have extensively examined the dependence of the scattering properties on volume fraction. The scattering coefficient shows a linear dependence in the dilute region up to approximately 5% of the volume fraction. This linear trend indicates that there is no interference between the scattered electric fields from particles, known as independent scattering [9,10,16]. Meanwhile, in the dense regime, the rate of increase is reduced, resulting in a curvilinear dependence on the volume fraction. This reduction suggests an enhancement of the destructive interference at far field between the scattered fields, known as the interference effect [13,17,18]. However, constructive interference can also occur, as in Young's double-slit experiment. Thus, it is plausible that the observed interference effect results from a combination of constructive and destructive contributions. However, their quantitative contributions remain unclear.

The dependent scattering theory (DST) nicely describes the measurement data of the scattering properties in dense suspensions up to approximately 25% [13,17,18]. This electromagnetic theory is based on the first-order solution of the Foldy–Lax equations, which provide a multiple-scattering expansion of Maxwell's equations [19,20]. The DST formulates the scattering coefficient as the integral of the product of the single-particle phase function and the static structure factor (SSF) over the scattering angle. The Mie theory provides the phase function, where the particle diameter is comparable to the wavelength, as a summation of special functions [21]. The SSF provides destructive and constructive interference contributions [13,18,22,23] and can be measured by neutron scattering techniques [24,25]. However, these interference contributions vary in a complicated manner with the scattering angle, wavelength, particle size, and other factors. Moreover, the SSF reflects the local particle configuration and a pair correlation between particles induced by particle interaction, such as the hard-sphere repulsion [26,27]. Quantitative understanding is hindered by both the complicated form of the phase function and the variation in the SSF.

We aim to clarify the two interference contributions on the light scattering properties in dense suspensions by a density expansion approach. The expansion approach was initially developed in physical chemistry to study the particle correlations using the radial distribution function (RDF) [28–31]. The RDF is related to the SSF as its inverse Fourier transform. Each order of the volume fraction (number density) links to the particle correlation, such as the excluded volume and effective attractive force. Despite its widespread use, to the best of our knowledge, the volume-fraction expansion approach has not been applied to the decomposition analysis of light-scattering properties, integrated over scattering angles. Thus, we also aim to clarify the relationship between interference and particle correlation. We calculated the scattering properties using the DST over a wide range of particle diameters (100–800 nm) and optical wavelengths (600–1000 nm). Then, we expanded the scattering properties in order of the volume fraction and examined the interference contributions and their relationship quantitatively.

2. Theory and model

2.1. Modeling colloidal suspensions

Among the light scattering properties, we mainly considered the scattering and reduced scattering coefficients, μ_s and μ_s'. The two coefficients characterize the scattering events at unit length in the ballistic and diffusive regimes (small and large scales), respectively, as shown in Fig. 1(a). Each diffusion process, characterized by μ_s', involves multiple ballistic scattering events characterized by μ_s.

We model the colloidal suspension as a system of spherical particles dispersed in a continuous solvent medium (water), as shown in Fig. 1(b). We focus on a monodisperse system with a particle diameter d. Examples of the actual systems are silica and polystyrene particles [18,32–34], whose size distributions are sufficiently sharp to hold the monodisperse approximation [35]. For simplicity, we assume that no agglomeration occurs in the system.

We carefully use the terms "independent" scattering and "dependent" scattering throughout this paper. Although their ambiguity has been noted [36], these terms are widely used in optics and engineering research. The DST used in this study is based on the first-order solution of the Foldy–Lax equations (FLEs), which provide a multiple-scattering expansion of Maxwell's equations [19,20].

2.2. Dependent scattering theory (DST)

The DST provides the formulations of the two scattering coefficients (incoherent properties) as integrals with respect to the scattering angle θ [17,18].

$$\mu_{s,DST}(d) = 2\pi n_0 \sigma_{s,Mie}(d) \int_0^\pi d\theta \sin\theta \hat{P}_{Mie}(\theta, d) S(\theta, d), \quad (1)$$

$$\mu'_{s,DST}(d) = 2\pi n_0 \sigma_{s,Mie}(d) \int_0^\pi d\theta \sin\theta (1 - \cos\theta) \hat{P}_{Mie}(\theta, d) S(\theta, d). \quad (2)$$

Here, the number density n_0 is given as η/v_m with the volume fraction η and particle volume $v_m = \pi d^3/6$. $\sigma_{s,Mie}$ and $\hat{P}_{Mie}$ are the single-particle scattering cross section and normalized phase function using the Mie theory [21]. $S(\theta, d)$ represents the static structure factor (SSF), which describes the interference between scattered electric fields from particles. The two coefficients depend on the volume fraction and optical wavelength λ, but we abbreviate the dependence here for simple notation.

The above formulations are based on an optics and engineering perspective. In optical measurements, the wavelength is typically selected in advance and colloidal samples with specified diameters are

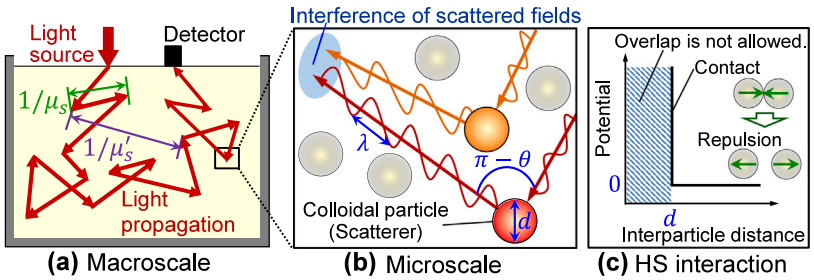

Fig. 1. Schematics of (a) light propagation on the macroscopic (centimeter) scale, (b) electromagnetic scattering on the microscopic (micrometer) scale in a monodisperse colloidal suspension, and (c) hard-sphere (HS) interaction between particles.

Table 1
Relationship of the volume fraction expansion between the RDF $g(r)$, SSF $S(\theta)$, and two scattering coefficients μ_s and μ_s', where the order index $j = 1, 2, 3, \ldots$ for the same treatment of the particle correlation.

	$g(r)$	$S(\theta)$	μ_s and μ_s'
Expansion order	$j-1$	j	$j+1$
Expansion coefficient	g_{j-1}	S_j	Q_j^s and Q_j^p
Interparticle correlation range	jd	–	–

used. Consequently, many studies examine the effects of wavelength and particle diameter on optical properties separately (e.g., [12]). Furthermore, optical measurement studies extensively investigate the dependence of scattering intensity on the scattering angle (e.g., [10]).

The DST results agree with FLEs' results in the current volume fraction range [19], indicating that the far-field interference, considered in this study, is the dominant contribution.

2.3. Static structure factor (SSF) and its volume fraction expansion

The SSF calculation requires a particle interaction model. Here, we employed the Percus–Yevick (PY) model [37,38], which is widely used for colloidal suspensions [26,27]. The PY model is one of the hard-sphere (HS) repulsion models, as shown in Fig. 1(c), and accounts for the indirect contributions of pair correlations through intermediate many-body effects [30]. The PY model would be the most reliable in colloidal systems without particle agglomeration because the DST with the PY model accurately describes the measurement data of the scattering properties at different volume fractions up to approximately 25% [18,33,34]. The analytical formulation of the SSF for the PY model is given as

$$S_{PY}(\eta, K) = 1/[1 + Y(\eta, K)], \tag{3}$$

where $K = 4\pi n_b d\lambda^{-1}\sin(\theta/2)$ with the refractive index of the background medium n_b. The explicit formulation of $Y(\eta, K)$ is referred to in [19,38].

We expand the SSF using the PY model in a series of the volume fraction, η

$$S_{PY}(\eta) \sim \sum_{j=0}^{N_e} S_j \eta^j = 1 + S_1\eta + S_2\eta^2 \cdots. \tag{4}$$

S_j is the expansion coefficient with $S_0 = 1$ and N_e is the maximum expansion order, which is theoretically infinity. The unity value of the SSF corresponds to no interference. In the S_j-calculation, we used two approaches: the cluster and Taylor expansion approaches. The former approach provides a physical interpretation between the particle correlation and interference, but its calculation is complicated especially at a high order. The latter approach enables the simple calculation, but it does not provide the physical interpretation. For systematic examination, this study used both approaches in a complementary manner.

2.3.1. Cluster expansion approach

In this subsection, we calculated S_j in Eq. (4) using the cluster expansion approach [28–31] up to the third order ($N_e = 3$). This approach is based on the radial distribution function (RDF), $g(\hat{r})$, with the particle distance $\hat{r} = r/d$ normalized by the particle diameter, as shown in Fig. 2(a). The RDF describes a pair correlation between particles and a local particle configuration induced by particle interaction. The Fourier transform of the RDF gives the SSF. As listed in Table 1, the expansion order of the RDF is one lower than that of the SSF for the same treatment of the particle correlation, because the SSF involves the volume integration. Thus, we expanded the RDF up to the second order,

$$g_{PY}(\hat{r}) = \Theta(\hat{r} - 1)\left[g_0 + \frac{6}{\pi}g_1(\hat{r})\eta + \frac{36}{\pi^2}g_2(\hat{r})\eta^2\right] + O(\eta^3). \tag{5}$$

The step function, $\Theta(\hat{r} - 1)$, comes from the Boltzmann factor with the HS potential and represents the excluded volume. The expansion coefficients, $g_0 = 1$, $g_1(\hat{r})$, and $g_2(\hat{r})$, represent the cluster integrals for the zeroth, first, and second orders.

The explicit form of g_1 for the PY model is given as [28]

$$\begin{aligned} g_1(\hat{r}_{12}) &= \int d\hat{\boldsymbol{r}}_3 f(\hat{r}_{13}) f(\hat{r}_{23}) \\ &= \frac{4\pi}{3}\left(1 - \frac{3}{4}\hat{r}_{12} + \frac{1}{16}\hat{r}_{12}^3\right)\left[1 - \Theta(\hat{r}_{12} - 2)\right]. \end{aligned} \tag{6}$$

Here, $f(\hat{r}_{kl}) = \Theta(\hat{r}_{kl} - 1) - 1$ represents the Mayer function with the HS potential, $\hat{r}_{kl}$ denotes the distance between Particle k and Particle l with $k = 1, 2, \ldots$ and $l = 2, 3, \ldots$, normalized by the diameter. The explicit labeling of particles clearly distinguishes the target particles (1 and 2) from the intermediate particles (the others). The cluster integral, g_1, is drawn by a graph or diagram in Fig. 2(b), and it involves the indirect effect via Particle 3: correlations between Particles 1–3 and Particles 2–3. From the function $1 - \Theta(\hat{r}_{12} - 2)$ in Eq. (6), g_1 represents the pair correlation for interparticle distances up to $2d$, as listed in Table 1. In the second-order expansion, the PY model treats the following two cluster integrals, represented as g_{2A} and g_{2B} [30]

$$\begin{aligned} g_2(\hat{r}_{12}) &= g_{2A}(\hat{r}_{12}) + g_{2B}(\hat{r}_{12}), \\ g_{2A}(\hat{r}_{12}) &= \int d\hat{\boldsymbol{r}}_3 \int d\hat{\boldsymbol{r}}_4 f(\hat{r}_{13}) f(\hat{r}_{24}) f(\hat{r}_{34}), \end{aligned} \tag{7}$$

$$g_{2B}(\hat{r}_{12}) = \int d\hat{\boldsymbol{r}}_3 \int d\hat{\boldsymbol{r}}_4 f(\hat{r}_{13}) f(\hat{r}_{23}) f(\hat{r}_{24}) f(\hat{r}_{34}). \tag{8}$$

The explicit forms of g_{2A} and g_{2B} are calculated as [29]

$$\begin{aligned} g_{2A}(\hat{r}_{12}) &= \pi^2\left[1 - \Theta(\hat{r}_{12} - 3)\right] \\ &\quad \times \left(-\frac{9}{4} + \frac{27}{70\hat{r}_{12}} + \frac{9}{5}\hat{r}_{12} - \frac{\hat{r}_{12}^2}{4} - \frac{\hat{r}_{12}^3}{6} + \frac{\hat{r}_{12}^4}{20} - \frac{\hat{r}_{12}^6}{1260}\right), \end{aligned} \tag{9}$$

$$\begin{aligned} g_{2B}(\hat{r}_{12}) &= 2\pi^2\left[1 - \Theta(\hat{r}_{12} - 2)\right] \\ &\quad \times \left(\frac{16}{9} - \frac{9}{35\hat{r}_{12}} - \frac{97}{60}\hat{r}_{12} + \frac{\hat{r}_{12}^2}{4} + \frac{\hat{r}_{12}^3}{6} - \frac{\hat{r}_{12}^4}{20} + \frac{\hat{r}_{12}^6}{1260}\right). \end{aligned} \tag{10}$$

The above expressions indicate that g_{2A} and g_{2B} represent the pair correlations for interparticle distances up to $3d$ and $2d$, respectively.

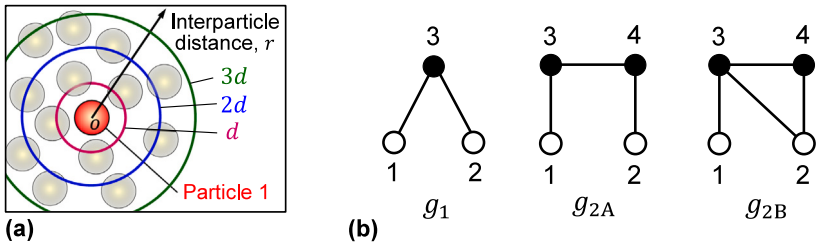

Fig. 2. (a) Schematic of pair correlation for interparticle distances. (b) Graph representation of the cluster integrals, g_1, g_{2A}, and g_{2B}. Open vertices indicate fixed particle positions, solid vertices represent integration over the position, and bonds denote the direct correlation via the Mayer function.

From the expansion coefficients of the RDF, g_{j-1} ($j = 1,2,3$), we obtained the expansion coefficient of the SSF, S_j, in the following,

$$\begin{aligned} S_1(K) &= \frac{24}{d^3}\int_0^\infty drr^2\left[\Theta(\hat{r}-1)g_0-1\right]\frac{\sin(Kr)}{Kr}, \\ S_2(K) &= \frac{24}{d^3}\frac{6}{\pi}\int_0^\infty drr^2\Theta(\hat{r}-1)g_1(\hat{r})\frac{\sin(Kr)}{Kr}, \\ S_3(K) &= \frac{24}{d^3}\left(\frac{6}{\pi}\right)^2\int_0^\infty drr^2\Theta(\hat{r}-1)g_2(\hat{r})\frac{\sin(Kr)}{Kr}. \end{aligned} \tag{11}$$

2.3.2. Taylor expansion approach

In the calculations of S_j (Eq. (4)), we employed the Taylor expansion of the SSF for the PY model (Eq. (3)),

$$\begin{aligned} S_1(K) &= \left.\frac{\partial S_{PY}}{\partial\eta}\right|_{\eta=0} = -Y_1, \\ S_2(K) &= \frac{1}{2}\left.\frac{\partial^2 S_{PY}}{\partial\eta^2}\right|_{\eta=0} = Y_1^2 - \frac{1}{2}Y_2, \\ S_3(K) &= \frac{1}{3!}\left.\frac{\partial^3 S_{PY}}{\partial\eta^3}\right|_{\eta=0} = -Y_1^3 + Y_1Y_2 - \frac{1}{6}Y_3, \\ S_4(K) &= \frac{1}{4!}\left.\frac{\partial^4 S_{PY}}{\partial\eta^4}\right|_{\eta=0} = Y_1^4 - \frac{3}{2}Y_1^2Y_2 + \frac{1}{4}Y_2^2 + \frac{1}{3}Y_1Y_3 - \frac{1}{24}Y_4. \end{aligned} \tag{12}$$

Here, we considered the expansion up to the fourth order ($N_e = 4$). The explicit formulations of Y_i ($i = 1,2,3,4$) are calculated as

$$\begin{aligned} Y_1(K) &= \left.\frac{\partial Y}{\partial\eta}\right|_{\eta=0} = \frac{24}{K^3}X_{1a}, \\ Y_2(K) &= \frac{1}{2}\left.\frac{\partial^2 Y}{\partial\eta^2}\right|_{\eta=0} = \frac{96}{K^3}(4X_{1a}-3X_{1b}) + \frac{24}{K^3}X_{2a}, \\ Y_3(K) &= \frac{1}{3!}\left.\frac{\partial^3 Y}{\partial\eta^3}\right|_{\eta=0} = \frac{72\cdot 60}{K^3}(X_{1a}-X_{1b}) + \frac{576}{K^3}X_{2a}, \\ Y_4(K) &= \frac{1}{4!}\left.\frac{\partial^4 Y}{\partial\eta^4}\right|_{\eta=0} = \frac{96}{K^3}(456X_{1a}-513X_{1b}) + \frac{144\cdot 60}{K^3}X_{2a}. \end{aligned} \tag{13}$$

X_{1a}, X_{1b}, and X_{2a} are given as

$$\begin{aligned} X_{1a}(K) &= \sin K - K\cos K, \\ X_{1b}(K) &= 2\sin K + \left(\frac{2}{K^2}-1\right)K\cos K - \frac{2}{K}, \\ X_{2a}(K) &= 4\left(1-\frac{6}{K^2}\right)\sin K - \left(1-\frac{12}{K^2}+\frac{24}{K^4}\right)K\cos K + \frac{24}{K^3}. \end{aligned} \tag{14}$$

We have preliminarily confirmed that the S_j-results obtained using the Taylor expansion approach are analytically equivalent to those obtained using the cluster expansion approach up to the third order.

2.4. Volume fraction expansion of the light scattering properties

Using the expansion results for the SSF (Eq. (4)), we obtained the expansion form of the scattering coefficient as

$$\mu_{s,exp} = m_s\eta\sum_{j=0}^{N_e}Q_j^s\eta^j = m_s\eta + m_sQ_1^s\eta^2 + m_sQ_2^s\eta^3\cdots, \tag{15}$$

$$Q_j^s = 2\pi\int_0^\pi d\theta\sin\theta\hat{P}_{Mie}S_j. \tag{16}$$

Here, $m_s = \sigma_{s,Mie}/v_m$ and $Q_0^s = 1$. We also obtained the form of the reduced scattering coefficient as

$$\mu'_{s,exp} = m_s\eta\sum_{j=0}^{N_e}Q_j^p\eta^j = m_sQ_0^p\eta + m_sQ_1^p\eta^2 + m_sQ_2^p\eta^3\cdots, \tag{17}$$

$$Q_j^p = 2\pi\int_0^\pi d\theta\sin\theta(1-\cos\theta)\hat{P}_{Mie}S_j. \tag{18}$$

Here, $Q_0^p = 1 - g_{Mie}$ with the anisotropic factor g_{Mie} using the Mie theory.

Q_j^s and Q_j^p are in the same expansion order of S_j for the SSF, as listed in Table 1. Meanwhile, the expansion order of the two scattering coefficients is higher than that of the SSF by unity from the forms of the above equations. The first-order expansion ($N_e = 0$) of the two scattering coefficients corresponds to the independent scattering theory (IST), which does not account for the interference.

2.5. Numerical methods and conditions

Numerical calculations of the two scattering coefficients and expansion coefficients require the following input parameters: the particle size (diameter), optical wavelength, refractive indices of the particle and background medium, and volume fraction. The volume fraction ranges from 0.1% to 25%, particle diameter ranges from 100 to 800 nm, and the wavelength ranges from 600 to 1000 nm (near-infrared region). The refractive indices of the particles and the background medium were set to 1.44 and 1.33, respectively, referring to typical values for particles and water [20], and for simplicity assuming no wavelength dependence. Our study's size parameter ($\pi\times$ diameter/wavelength in a medium) ranges from 0.4 to 5.6, where the Mie scattering is dominant in the single-particle scattering.

About the DST calculation procedure, please refer to our previous study [20]. In the numerical calculations of S_j, we employed the formulations of Eq. (12) instead of using Eq. (11) to avoid possible numerical oscillation in the Fourier transform [39]. In the calculations of Q_j^s and Q_j^p (Eqs. (16) and (18)), we used the extended trapezoidal rule.

3. Results and discussion

3.1. SSF and RDF

Before examination of the light scattering properties, we examined the relation between the interference and particle correlation by the volume fraction expansion of the SSF and RDF (Eqs. (4) and (5)) in Fig. 3. The values of unity represent no particle correlation in the RDF and no interference in the SSF (Fig. 3(a)). As shown in Fig. 3, the PY results reflect many-body correlations in the RDF and multiple interference contributions in the SSF. However, the shapes of the results do not explicitly reveal the contributions of correlation and interference. To extract the relationship between them, we employ volume-fraction decomposition. Here, we plot the SSF as a function of the scattering angle, following the formulations of the two scattering coefficients in the DST (Eqs. (1) and (2)) from an optics and engineering perspective.

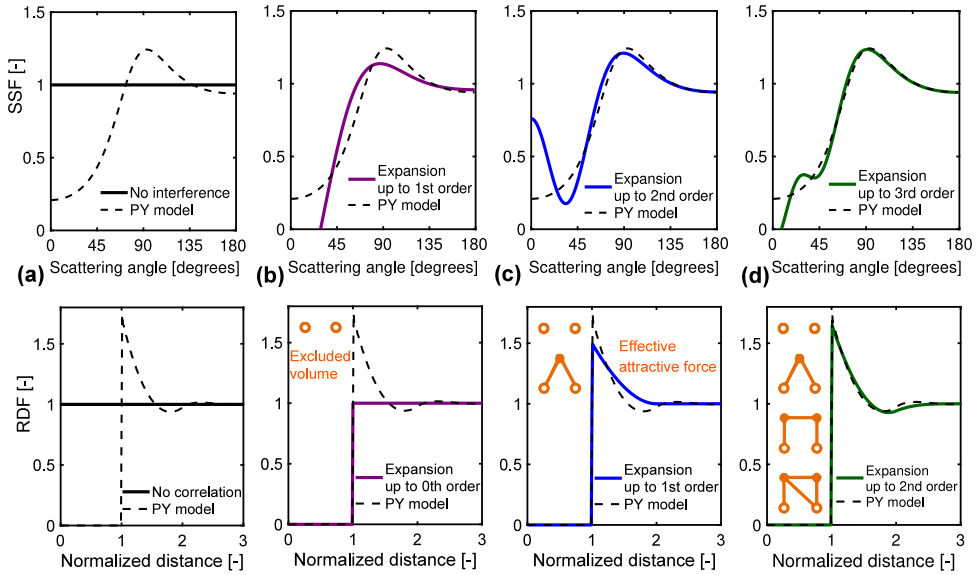

Fig. 3. Volume-fraction expansion of the SSF (top figures) and RDF (bottom figures) using the PY model at the volume fraction of 20%, particle diameter of 300 nm, optical wavelength of 600 nm. The expansion of the SSF up to the N_eth order corresponds to that of the RDF up to the $(N_e - 1)$th order for the same treatment of particle correlation, as listed in Table 1.

In physical chemistry, however, the K variable is typically used for a unified description. In either representation, the conclusions of our discussion remain unchanged.

The zeroth-order expansion of the RDF (bottom of Fig. 3(b)), that is, $g_0\Theta(\hat{r}-1)$, is known as the Debye model or gas model [40]. This model treats the excluded volume at the normalized distance less than unity, where the other particle is not allowed to exist. Correspondingly, destructive interference appears in the first-order expansion of the SSF (top of Fig. 3(b)), that is, $1 + S_1\eta$, for the scattering angle region of $0 < \theta \lesssim 45°$, where the SSF values are less than unity. The first-order term in the RDF expansion (bottom of Fig. 3(c)) includes an effective attractive contribution arising from a three-body correlation (Eq. (6)), even in the absence of any direct attractive force [28,30]. The RDF values are higher than unity in the region of $1 < \hat{r} < 2$, meaning particles are closely packed together by the effective attraction. The effective attractive contribution results in increasing the SSF values at small scattering angles ($0 < \theta \lesssim 30°$) in the top figure (c), representing an enhancement of the constructive interference. Such an increase in the SSF values at small scattering angles also appears in the sticky HS model, which accounts for the direct attractive interaction between particles [23,41], even though this model differs from the HS model considered in this study. In the SSF expansion (top of Fig. 3(c)), the peak position and value at $\theta \sim 90°$ become closer to the PY results compared to the first-order expansion (top of Fig. 3(b)). Fig. 3(d) shows that the RDF expansion to the second order and the SSF expansion to the third order closely match the PY model results, indicating that these orders provide the dominant contributions, where the interparticle distance for pair correlation is up to $3d$.

The SSF results include both destructive and constructive interference contributions as a function of the scattering angle. Meanwhile, the light scattering properties using the DST include two interference contributions, averaged over the scattering angles (Eqs. (1) and (2)), as discussed in the following subsection.

3.2. Light scattering properties

In this subsection, we examined the interference effect on the two scattering coefficients by their volume-fraction expansions (Eqs. (15) and (17)) with the expansion coefficients (Eqs. (16) and (18)). Here, the DST is the most accurate model without expansion, as the theory provides an excellent agreement with measurement data. Against the DST, we investigated a relative difference (RD), which is defined as

$$RD(Expansion) = [NR(DST) - NR(Expansion)]/NR(DST), \tag{19}$$

where $NR(DST)$ and $NR(Expansion)$ are the numerical results of the DST and expansions at each volume fraction.

Figs. 4(a) and (b) show the volume-fraction dependencies in the particle diameter of 100 nm (small size case) and wavelength of 600 nm. The orange-shaded area indicates the RD region, corresponding to a ±10% range from the DST results. The first-order expansion results ($\mu_s = m_s\eta$ and $\mu_s' = m_s Q_0^p \eta$), corresponding to the IST, are linear in the volume fraction because the SSF values are unity (top of Fig. 3(a)), indicating no interference. In the volume fraction range smaller than 3%, the first-order expansion agrees with the DST results to within ±10% RD.

Meanwhile, the expansions up to higher orders show curvilinear trends due to interference contributions. Higher-order expansion results tend to agree with the DST results over a broader range of volume fractions. In Fig. 4(b), the agreement ranges for the second through fifth-order expansions are up to approximately 11%, 16%, 19%, and 22% of the volume fraction, respectively. These results suggest that for small diameters, the DST results include multiple interference contributions induced by indirect contributions from the pair correlation through intermediate many-body effects.

Figs. 4(c) and (d) show the results for the two coefficients at a diameter of 600 nm (large size case). Compared to the small-diameter case, the lower-order expansion results agree with the DST across the entire volume fraction range; the third-order expansion is sufficient for the scattering coefficient, and the second-order expansion is adequate for the reduced scattering coefficient. These results suggest that the higher-order contributions from pair correlation and interference have a small impact on both scattering coefficients for a large diameter. From the perspective of expansion convergence, the large-diameter case shows fast convergence as the expansion order increases. Although not shown here, for the smaller-diameter case ($d = 100$ nm), the expansion results up to sixth order ($N_e = 5$) are within 10% of the DST results, indicating slower convergence. Further investigation into the quantitative convergence trends will be the subject of future work.

In Fig. 5, we investigated the absolute values of the RD for the second- and third-order expansions in the two scattering coefficients

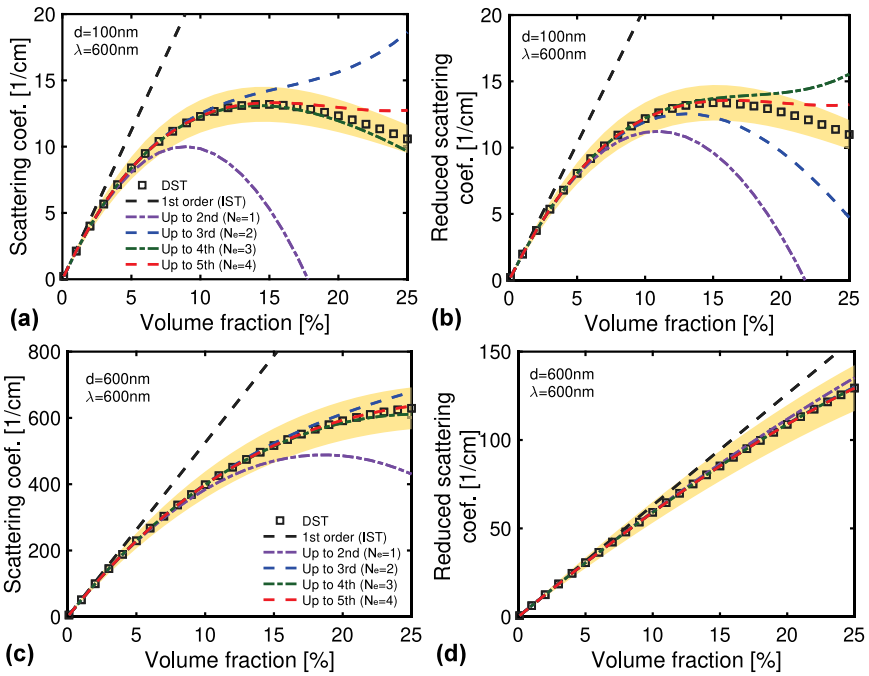

Fig. 4. Volume-fraction dependence of the two scattering coefficients in the wavelength of 600 nm and particle diameters of 100 and 600 nm (size parameters of 0.7 and 4.2): the DST (Eqs. (1) and (2)) and expansions (Eqs. (15) and (17)) up to different orders ($N_e + 1$). The orange-shaded area represents the region of the relative difference (RD), corresponding to a ±10% range from the DST results.

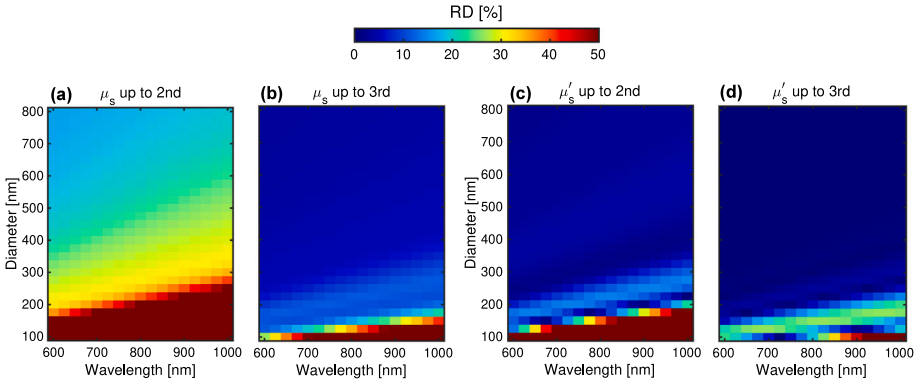

Fig. 5. Absolute values of the RD between the DST and expansion results up to the second and third orders in the scattering and reduced scattering coefficients (μ_s and μ_s') with a volume fraction of 20% at different wavelengths and diameters.

at different wavelengths and diameters with a volume fraction of 20%. Here, the RD values greater than 50 were capped at 50 to ensure clarity in the plots. All four cases demonstrated that the RD values strongly depend on the wavelength within the diameter range of 100–300 nm. In the other diameter range, however, the RD values are less dependent on the wavelength. Here, we discuss the RD results by the diameter rather than the wavelength.

Fig. 5(a) shows that the RD values for the second-order expansion exceed 20%, even over a large diameter range. This indicates that the second-order approximation does not accurately describe the scattering coefficient. In contrast, the third-order results in Fig. 5(b) show that the RD values are below 10% for diameters larger than approximately 300 nm, suggesting that the third-order approximation is valid for the scattering coefficient. Figs. 5(c) and (d) show that the RD values for both the second- and third-order results of the reduced scattering coefficient are below 10% for diameters larger than approximately 300 nm. These results suggest that the second-order approximation adequately describes the interference contributions. The second- and third-order expansions account for the contributions of the excluded volume and the effective attractive force, respectively. While the scattering coefficient mainly reflects both contributions, the reduced scattering coefficient primarily reflects the excluded volume contribution.

3.3. Expansion coefficients of the two scattering coefficients

As shown in Fig. 4(a), at high volume fractions, the second-order expansions are smaller than the first-order expansions (IST with no interference treatment). This result suggests that the expansion coefficient of Q_1^s is negative, meaning the destructive interference contribution. Also, the larger values of the third-order expansion than the second-order expansion indicate the positive value of Q_2^s with the constructive interference contribution. Here, we examine the expansion terms of $Q_j^s \eta^j$ and $Q_j^p \eta^j$ in Fig. 6, rather than considering the expansion coefficients alone. As shown in the expansion forms of the two scattering coefficients (Eqs. (15) and (17)), each term is the product of the expansion coefficient and the power η^j.

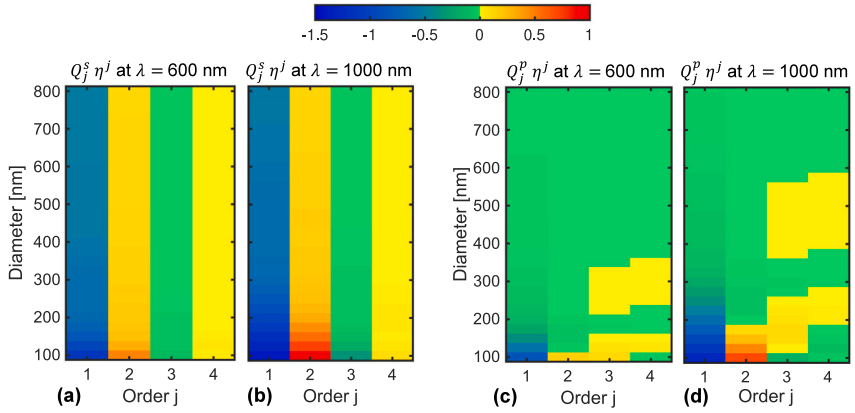

Fig. 6. Expansion terms, $Q_j^s\eta^j$ and $Q_j^p\eta^j$, of the scattering and reduced scattering coefficients (Eqs. (16) and (18)) at different orders and diameters with the wavelengths of 600 nm and 1000 nm (the size-parameter ranges of 0.7–5.6 and 0.4–3.3) for $\eta = 0.2$.

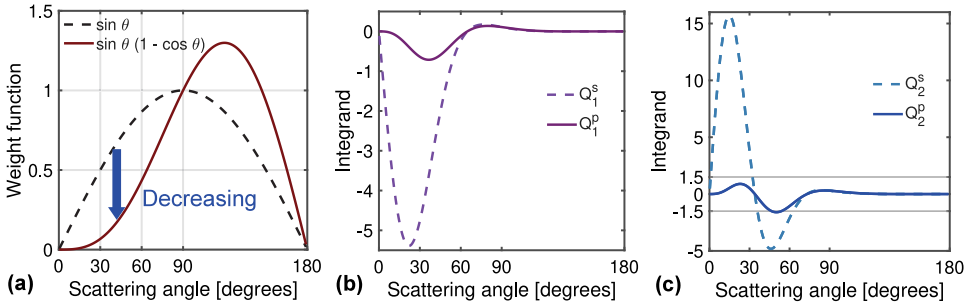

Fig. 7. Integrands of the expansion coefficients, Q_j^s and Q_j^p, as a function of the scattering angle θ at the particle diameter of 300 nm and the wavelength of 600 nm. (a) Weight functions, (b) the first-order expansion case, and (c) the second-order expansion case. Here, the integration values over the scattering angle are $Q_1^s = -3.14$ (negative), $Q_1^p = -0.32$ (slightly negative), $Q_2^s = 4.02$ (positive), and $Q_2^p = -0.23$ (slightly negative).

Figs. 6(a) and (b) show the diameter dependence of the expansion terms for the scattering coefficient up to the fourth order at wavelengths of 600 nm and 1000 nm, respectively. Here, cool and warm colors represent negative and positive values, respectively, and η is set as 0.2. The $Q_j^s\eta^j$ values are negative for odd orders and positive for even orders, indicating that the odd- and even-order terms contribute as destructive and constructive interference, respectively. In the diameter region smaller than approximately 300 nm, the results at each order vary with diameter, whereas in the larger diameter region, they remain nearly constant. The diameter dependence of the expansion terms explains the trend of the scattering coefficient expansion, as shown in Figs. 5(a) and (b). At higher orders, the $Q_j^s\eta^j$ values become smaller, indicating that the expansion is approaching convergence. Figs. 6(c) and (d) show that the $Q_j^p\eta^j$ results exhibit different trends in expansion order compared with the $Q_j^s\eta^j$ results, except for the first-order case. For instance, at a wavelength of 1000 nm, the $Q_2^p\eta^2$ values are positive in the diameter region smaller than 175 nm but negative in the larger diameter region. In contrast, the $Q_2^s\eta^2$ values remain positive throughout. The $Q_j^p\eta^j$ values are slightly negative across a wide range of orders and diameters, indicating that destructive interference predominates in the reduced scattering coefficient over constructive interference.

We investigate the reason behind the difference in expansion order trends between Q_j^s and Q_j^p by analyzing their integrands (i.e., the right-hand sides of Eqs. (16) and (18)) as functions of the scattering angle θ. We focus on the first- and second-order results for a diameter of 300 nm and a wavelength of 600 nm. The difference in the integrands between Q_j^s and Q_j^p lies in the weight function. As shown in Fig. 7(a), the weight function, $\sin\theta(1-\cos\theta)$, in the integrand of Q_j^p peaks at a larger scattering angle than $\sin\theta$ in the integrand of Q_j^s, due to the half-angle identity $1-\cos\theta = 2\sin^2(\theta/2)$. This peak shift significantly reduces the integrand (the product of $\hat{P}_{Mie}S_j$ and the weight function) in the forward-scattering region ($0 < \theta \lesssim 30°$), and moderately in the intermediate angle range ($30° \lesssim \theta \lesssim 60°$). As shown in Fig. 7(b), the prominent negative peak in the integrand of Q_1^s at $\theta \sim 22°$ becomes suppressed in the integrand of Q_1^p due to the difference in the weight functions. This suppression leads to a decrease in the Q_1^p value (obtained via integration over the scattering angle) compared to the Q_1^s value. Fig. 7(c) shows that the integrand of Q_2^s exhibits a positive peak at $\theta \sim 15°$, originating from the SSF peak in the forward scattering region, which represents the effective attractive contribution, as shown in Fig. 3(c). This positive peak in the integrand of Q_2^s is significantly reduced to less than 1.5 in the integrand of Q_2^p, owing to the weight function. Meanwhile, the negative peak at $\theta \sim 45°$ in the integrand of Q_2^s is only moderately reduced in the integrand of Q_2^p, remaining greater than 1.5. Consequently, the value of Q_2^p is slightly negative (−0.23), whereas that of Q_2^s is positive (4.02).

3.4. Examination of the experimental data

Finally, we apply the developed decomposition approach to experimental data from monodisperse colloidal suspensions. We used data of silica and polystyrene particles suspended in water, specifically for the scattering and reduced scattering coefficients, as reported by J. D. Nguyen et al. [18] and L. Bressel et al. [13], respectively, as shown in Fig. 8. In the numerical calculations, the refractive indices of silica and polystyrene were set to 1.44 at a wavelength of 1297 nm and 1.57 at 982 nm, respectively, based on the corresponding references.

The top panels of Fig. 8 show that the DST predictions agree well with the measured scattering and reduced scattering coefficients across the entire volume fraction range. In all cases except for case (c), the expansion results up to the fourth order ($N_e = 3$) show good agreement with both the measurement data and the DST results. This observation

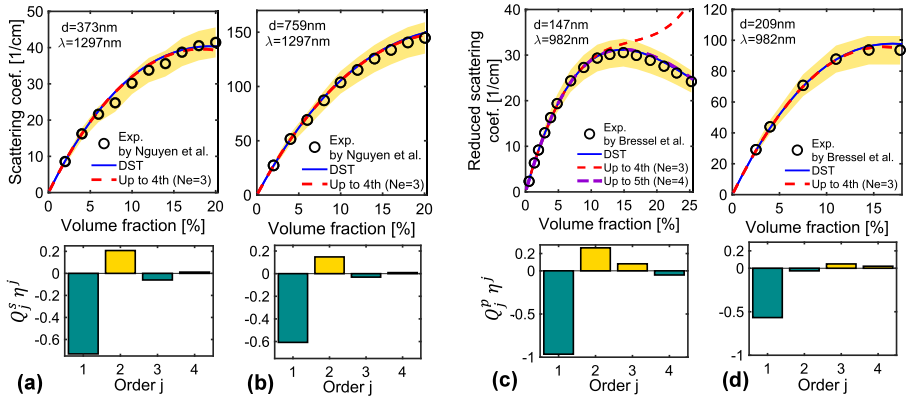

Fig. 8. Investigation of experimental data at the two diameter cases: (a) and (b) silica particles in water suspensions for the scattering coefficient by J. D. Nguyen et al. [18], (c) and (d) polystyrene particles in water suspensions for the reduced scattering coefficient by L. Bressel et al. [13]. (Top) Dependence on volume fraction. The orange-shaded area indicates the RD region within 10% deviation from the measurement data. (Bottom) Expansion terms. The other details are the same as in Figs. 4 and 6.

suggests that the dominant interference contributions are captured in the $N_e = 3$ case, and that the dominant pair correlation occurs at inter-particle distances up to $3d$. In case (c), however, a fifth-order expansion is required to achieve agreement with the measurement data. This case corresponds to a small-diameter condition, where multiple interference contributions become more significant, as discussed in Figs. 4(a) and (b). The bottom panels of the figure show that the absolute values of the expansion terms are larger for the smaller-diameter cases ((a) and (c)) than for the larger-diameter cases ((b) and (d)). In case (c), the absolute values are the largest among all cases, indicating the most significant interference contributions. The expansion-order dependence of $Q_j^p \eta^j$ is more complex, particularly in the second and third orders, compared to the more regular behavior observed in the $Q_j^s \eta^j$ results.

4. Conclusions

We investigated the far-field interference effects on the light scattering properties of concentrated colloidal suspensions by decomposing these properties through a volume fraction expansion. We calculated the two scattering coefficients using the DST with hard-sphere interaction and series expansions up to the fifth order over volume fractions ranging from 0.1% to 25%, particle diameter from 100 to 800 nm, and wavelengths from 600 to 1000 nm. Our numerical calculations show that, for the reduced scattering coefficient, the second-order expansion agrees well with the DST results for particle diameters larger than approximately 300 nm. This result indicates that the dominant contribution arises from destructive interference due to the excluded volume between particles, a manifestation of particle correlations. For the scattering coefficient, the third-order expansion agrees with the DST results in the larger-diameter region. This agreement reveals a hidden constructive-interference contribution arising from the effective attractive force, even in the absence of a direct attractive force. For smaller diameters, higher-order expansions are required to accurately reproduce the DST results, due to the involvement of multiple interference effects in both scattering coefficients. For the scattering coefficient, odd-order terms of expansion correspond to destructive interference, while even-order terms correspond to constructive interference. In contrast, the correspondence in the reduced scattering coefficient is more complex and depends on both particle diameter and wavelength due to the weight function. The developed decomposition approach can be applied to measured light scattering data to analyze multiple interference contributions.

As a future direction, it is important to extend the developed approach to other colloidal systems, such as polydisperse suspensions [42] and agglomerated systems involving direct attractive forces between particles. Among the electromagnetic theories for colloidal systems, effective medium approximations (EMAs; mixing rules) have also been widely employed. The EMAs can be derived from the FLEs via the Born series [43,44]. This fact implies a relationship between the EMAs and the DST, as well as the possibility of applying the volume-fraction expansion to the EMAs. Exploring this possibility remains a challenging task for future research. Another direction for future work is to investigate interference contributions under conditions in which FLEs or full-wave calculations [45] are required instead of the DST, such as in super-dense suspensions or for particles with high refractive indices.

Our findings offer a quantitative understanding of interference effects on light scattering properties, which could not be fully analyzed by DST calculations alone [13,17,18]. They also contribute fundamental insights toward the development of nanotechnological methods for non-destructive evaluation of particle properties using scattered light.

CRediT authorship contribution statement

Hiroyuki Fujii: Writing – original draft, Software, Investigation, Funding acquisition, Conceptualization. **Sou Sasaki:** Writing – review & editing, Software, Methodology, Investigation, Formal analysis. **Ryuga Sawada:** Writing – review & editing, Investigation, Formal analysis, Conceptualization. **Kazumichi Kobayashi:** Writing – review & editing, Supervision. **Masao Watanabe:** Writing – review & editing, Supervision.

Declaration of generative AI and AI-assisted technologies in the manuscript preparation process

During the preparation of this work, the authors used "Grammarly" in order to improve language and readability. After using this tool/service, the authors reviewed and edited the content as needed and take full responsibility for the content of the published article.

Declaration of competing interest

The authors declare the following financial interests/personal relationships which may be considered as potential competing interests: Hiroyuki Fujii reports financial support was provided by Japan Society for the Promotion of Science. Hiroyuki Fujii reports financial support was provided by Leave a Nest. If there are other authors, they declare that they have no known competing financial interests or personal relationships that could have appeared to influence the work reported in this paper.

Acknowledgments

We would like to thank Prof. Dr. G. Nishimura, Prof. Dr. K. B. Bec, Prof. Dr. A. Ikehata, Prof. Dr. J. Dyre, Prof. Dr. N. Oshima, and Mr. T. Aoki for their valuable comments from both theoretical and experimental points of view. The first author (H.F.) acknowledges financial support from JST PRESTO, Japan (JPMJPR25J8), Grant -in-Aid for Scientific Research, Japan (22KK0243, 25K02127) of JSPS, KAKENHI, the Leave a Nest Grant (Nipponham award), and the f3 Engineering Education and Research Center, Faculty of Engineering, Hokkaido University, Japan.

Data availability

Data will be made available on request.

References

[1] F. Bonacci, X. Chateau, E.M. Furst, J. Fusier, J. Goyon, A. Lemaître, Contact and macroscopic ageing in colloidal suspensions, Nat. Mater. 19 (2020) 775–780, http://dx.doi.org/10.1038/s41563-020-0624-9.

[2] T.G. Slavova, G.M. Radulova, P.A. Kralchevsky, K.D. Danov, Encapsulation of fragrances and oils by core–shell structures from silica nanoparticles, surfactant and polymer: Effect of particle size, Colloids Surf. A 606 (2020) 125558, 1–11.

[3] J. Chun, T. Oh, M. Luna, M. Schweiger, Effect of particle size distribution on slurry rheology: Nuclear waste simulant slurries, Colloids Surf. A: Physicochem. Eng. 384 (2011) 304–310, http://dx.doi.org/10.1016/j.colsurfa.2011.04.003.

[4] R. Studart, E. Amstad, L.J. Gauckler, Colloidal stabilization of nanoparticles in concentrated suspensions, Langmuir 23 (18) (2007) 1081–1090, http://dx.doi.org/10.1021/la062042s.

[5] M. Shimoyamada, A. Ishiyama, H. Masuda, S. Egusa, M. Matsuno, Viscosity changes of soymilk due to vacuum evaporation with moderate heating, LWT - Food Sci. Technol. 112 (108255) (2019) 1–7, http://dx.doi.org/10.1016/j.lwt.2019.108255.

[6] G.L. Hunter, E.R. Weeks, The physics of the colloidal glass transition, Rep. Progr. Phys. 75 (066501) (2012) 1–30, http://dx.doi.org/10.1088/0034-4885/75/6/066501.

[7] J.C. Dyre, Simple liquids' quasiuniversality and the hard-sphere paradigm, J. Phys.: Condens. Matter. 28 (323001) (2016) 1–22, http://dx.doi.org/10.1088/0953-8984/28/32/323001.

[8] J. Knorr, J. Cui, T.M. Koller, A.P. Fröba, Evaluation strategy towards an accurate determination of viscosity and interfacial tension by surface light scattering in presence of line- broadening effects, J. Colloid Interface Sci. 623 (2022) 595–606, http://dx.doi.org/10.1016/j.jcis.2022.05.043.

[9] C. Li, H. Jiang, Imaging of particle size and concentration in heterogeneous scattering media using multispectral diffuse optical tomography, Opt. Express 12 (25) (2004) 6313–6318, http://dx.doi.org/10.1364/OPEX.12.006313.

[10] R. Michels, F. Foschum, A. Kienle, Optical properties of fat emulsions, Opt. Express 16 (8) (2008) 5907–5925, http://dx.doi.org/10.1364/OE.16.005907.

[11] Y. Hemar, W. Banjar, D. Otter, Z. Yang, Viscosity, size, structural and interfacial properties of sodium caseinate obtained from A2 milk, Colloids Surf. A: Physicochem. Eng. 614 (126163) (2021) 1–6, http://dx.doi.org/10.1016/j.colsurfa.2021.126163.

[12] R. Borah, S.W. Verbruggen, Effect of size distribution, skewness and roughness on the optical properties of colloidal plasmonic nanoparticles, Colloids Surf. A: Physicochem. Eng. 640 (2022) 128521, http://dx.doi.org/10.1016/j.colsurfa.2022.128521.

[13] L. Bressel, R. Hass, O. Reich, Particle sizing in highly turbid dispersions by photon density wave spectroscopy, J. Quant. Spectrosc. Radiat. Transfer 126 (2013) 122–129, http://dx.doi.org/10.1016/j.jqsrt.2012.11.031.

[14] A.K. Van Helden, A. Vrij, Static light scattering of concentrated silica dispersions in apolar solvents, J. Colloid Interface Sci. 78 (2) (1980) 312–329, http://dx.doi.org/10.1016/0021-9797(80)90570-6.

[15] V. Ntziachristos, Going deeper than microscopy: The optical imaging frontier in biology, Nat. Methods 7 (8) (2010) 603–614, http://dx.doi.org/10.1038/nmeth.1483.

[16] H.J. van Staveren, C.J.M. Moes, J. van Marie, S.A. Prahl, M.J.C. van Gemert, Light scattering in intralipid-10 % in the wavelength range of 400-1100 nm, Appl. Opt. 30 (31) (1991) 4507–4514, http://dx.doi.org/10.1364/AO.30.004507.

[17] J.D. Cartigny, Y. Yamada, C.L. Tien, Radiative transfer with dependent scattering by particles: part 1 - theoretical investigation, J. Heat Transf. 108 (1986) 608–613, http://dx.doi.org/10.1115/1.3246979.

[18] V.D. Nguyen, D.J. Faber, E. van der Pol, T.G. van Leeuwen, J. Kalkman, Dependent and multiple scattering in transmission and backscattering optical coherence tomography, Opt. Express 21 (24) (2013) 29145–29156, http://dx.doi.org/10.1364/OE.21.029145.

[19] L. Tsang, J.A. Kong, K.-H. Ding, C.O. Ao, Scattering of Electromagnetic Waves: Numerical Simulations, John Wiley & Sons, Ltd, 2001.

[20] H. Fujii, L. Tsang, J. Zhu, K. Nomura, K. Kobayashi, M. Watanabe, Photon transport model for dense polydisperse colloidal suspensions using the radiative transfer equation combined with the dependent scattering theory, Opt. Express 28 (15) (2020) 22962–22977, http://dx.doi.org/10.1364/OE.398582.

[21] C.F. Bohren, D.R. Huffman, Absorption and Scattering of Light By Small Particles, John Wiley & Sons, 1983.

[22] A. Vrij, J.W. Jansen, J.K. Dhont, C. Pathmamanoharan, M.M. Kops-Werkhoven, H.M. Fijnaut, Light scattering of colloidal dispersions in non-polar solvents at finite concentrations: Silica spheres as model particles for hard-sphere interactions, Faraday Discuss. Chem. Soc. 76 (1983) 19–35, http://dx.doi.org/10.1039/DC9837600019.

[23] L.X. Ma, C.C. Wang, J.Y. Tan, Light scattering by densely packed optically soft particle systems, with consideration of the particle agglomeration and dependent scattering, Appl. Opt. 58 (27) (2019) 7336–7345, http://dx.doi.org/10.1364/AO.58.007336.

[24] M.H. Duits, R.P. May, A. Vrij, C.G. de Kruif, Small-angle neutron scattering of concentrated adhesive-hard-sphere dispersions, Langmuir 7 (1) (1991) 62–68, http://dx.doi.org/10.1021/la00049a014.

[25] A.T. Woutersen, R.P. May, C.G. de Kruif, The equilibrium microstructure of adhesive hard sphere dispersions: A small-angle neutron scattering study, J. Colloid Interface Sci. 151 (2) (1992) 410–420, http://dx.doi.org/10.1016/0021-9797(92)90490-D.

[26] D. Henderson, An explicit expression for the solvent contribution to the force between colloidal particles using a hard sphere model, J. Colloid Interface Sci. 121 (2) (1988) 486–490.

[27] F. Dekker, B.W.M. Kuipers, Á.G. García, R. Tuinier, A.P. Philipse, Scattering from colloidal cubic silica shells : Part II, static structure factors and osmotic equation of state, J. Colloid Interface Sci. 571 (2020) 267–274, http://dx.doi.org/10.1016/j.jcis.2020.02.058.

[28] J.G. Kirkwood, Statistical mechanics of fluid mixtures, J. Chem. Phys. 3 (5) (1935) 300–313.

[29] B.R. Nijboer, L. Van Hove, Radial distribution function of a gas of hard spheres and the superposition approximation, Phys. Rev. 85 (5) (1952) 777–783, http://dx.doi.org/10.1103/PhysRev.85.777.

[30] R. Balescu, Equilibrium and Nonequilibrium Statistical Mechanics, Wiley, New York, 1975.

[31] J.-P. Hansen, I. McDonald, Theory of Simple Liquids, Elsevier, 2006.

[32] Y. Yamada, J.D. Cartigny, C.L. Tien, Radiative transfer with dependent scattering by particles: part 2 - experimental investigation, J. Heat Transf. 108 (1986) 614–618, http://dx.doi.org/10.1115/1.3246980.

[33] S. Fraden, G. Maret, Multiple light scattering from concentrated, interacting suspensions, Phys. Rev. Lett. 65 (4) (1990) 512–515, http://dx.doi.org/10.1103/PhysRevLett.65.512.

[34] L.F. Rojas-Ochoa, S. Romer, F. Scheffold, P. Schurtenberger, Diffusing wave spectroscopy and small-angle neutron scattering from concentrated colloidal suspensions, Phys. Rev. E 65 (2002) 1–8, http://dx.doi.org/10.1103/PhysRevE.65.051403, 051403.

[35] H. Fujii, H. Na, J. Yi, K. Kobayashi, M. Watanabe, Particle size distribution effects on the light scattering properties in non-diluted colloidal suspensions: A numerical study, Colloids Surf. A: Physicochem. Eng. 703 (135208) (2024) 1–9, http://dx.doi.org/10.1016/j.colsurfa.2024.135208.

[36] M.I. Mishchenko, Independent and dependent scattering by particles in a multi-particle group, OSA Contin. 1 (1) (2018) 243–260, http://dx.doi.org/10.1364/OSAC.1.000243.

[37] J.K. Percus, G.J. Yevick, Analysis of classical statistical mechanics by means of collective coordinates, Phys. Rev. 110 (1) (1958) 1–13, http://dx.doi.org/10.1103/PhysRev.110.1.

[38] R.J. Hunter, Foundations of Colloid Science, Oxford University Press Inc., New York, 2001.

[39] J.S. Hansen, Nanoscale Hydrodynamics of Simple Systems, Cambridge University Press, 2022.

[40] P. Debye, Über die Zerstreuung von Röntgenstrahlen an amorphen Körpern, Phys. Z 28 (1927) 135–141.

[41] H. Fujii, K. Nishikawa, H. Na, K. Kobayashi, M. Watanabe, Polydisperse stickiness and particle size on light scattering in dense colloidal suspensions : A numerical study using the binary sticky hard-sphere model, Results Phys. 73 (2025) 108247, http://dx.doi.org/10.1016/j.rinp.2025.108247.

[42] W.L. Griffith, R. Triolo, A.L. Compere, Analytical structure function of a polydisperse percus–yevick fluid with schulz- (Gamma-) distributed diameters, Phys. Rev. A 35 (5) (1987) 2200–2206, http://dx.doi.org/10.1103/PhysRevA.33.2197.

[43] P. Mallet, C.A. Guérin, A. Sentenac, Maxwell–Garnett mixing rule in the presence of multiple scattering : Derivation and accuracy, Phys. Rev. B 72 (014205) (2005) 1–9, http://dx.doi.org/10.1103/PhysRevB.72.014205.

[44] C.A. Guérin, P. Mallet, A. Sentenac, Effective-medium theory for finite-size aggregates, J. Opt. Soc. Amer. A 23 (2) (2006) 349–358, http://dx.doi.org/10.1364/JOSAA.23.000349.

[45] K. Muinonen, J. Markkanen, T. Väisänen, J. Peltoniemi, A. Penttilä, Multiple scattering of light in discrete random media using incoherent interactions, Opt. Lett. 43 (4) (2018) 683–686, http://dx.doi.org/10.1364/OL.43.000683.